A MODEL FOR PREDICTING THE CURED PART THICKNESS OF AUTOMATED FIBER PLACED COMPOSITES

Matthew L. Kirby[a], Christopher J. Madsen[b], David S. Riha[a], Christopher T. Palmer[b], Paul F. Olsen[b]

[a]Southwest Research Institute
San Antonio, Texas

[b]Northrop Grumman Innovation Systems
Clearfield, Utah

ABSTRACT

Fabricating polymer matrix composite parts within a tight thickness tolerance can be a significant challenge due to incoming material and part-manufacturing variability. Predicting part thickness prior to cure based on incoming material and process parameters may provide an opportunity to apply pre-cure ply compensation in order to achieve the desired post-cure thickness. Recently a model was developed to predict the cured thickness of composite parts fabricated via a hand layup process. This thickness model was demonstrated for hand layup unidirectional tape composite parts, but the model does not capture the unique variations and uncertainties associated with automated fiber placed parts, namely the reduction in prepreg areal weight due to tape slitting. Since the automated fiber placement process offers increased material deposition rates along with reduced material waste, many composite part-manufacturing operations are moving to automated fiber placement. Therefore, it is necessary to develop capabilities to predict the thickness of automated fiber placed parts. The goals of this work were to (1) calibrate the thickness model for automated fiber placed composite parts and (2) validate the thickness predictions for production-scale representative parts. Additionally, prepreg areal weight monitoring methods were investigated to improve model predictions.

1. INTRODUCTION

Manufacturing processes for polymer matrix composites consist of a number of sources of variability and uncertainty, which lead to considerable variability in part thickness [1, 2]. Prepreg areal weight (PPAW), vacuum debulk, and resin flow/resin bleed during consolidation and cure have been shown to be the most significant sources of variability in part thickness [3]. Design constraints for advanced composites, especially those used in aerospace applications, often involve tight thickness tolerances. For high-performance aerospace programs, thickness tolerances can be as tight as $\pm 1.5\%$. The combination of tight thickness tolerances and significant part thickness variability results in many parts needing rework or thickness compensation to meet specification. Ultimately, these corrective actions add time to the manufacturing schedule and increase the cost of the final part. These issues were addressed in a related study for hand layup autoclave composite fabrication with the development of a model that predicts the post-cure thickness prior to cure, thus paving the way for pre-cure ply compensation and the elimination of the more costly post-

SAMPE Conference Proceedings. Charlotte, NC, May 20-23, 2019. Society for the Advancement of Material and Process Engineering – North America.

cure ply compensation process [3]. Although the model still needs quantitative validation, it captured trends in thickness and thickness variability for thin flat panels. However, increasingly the aerospace industry has been moving away from hand layup fabrication towards automated manufacturing methods, in order to increase production rates and reduce technician-to-technician process variability [4, 5]. Thus, the goal of this research was to extend the thickness model previously developed for hand layup fabrication to predict the thickness of automated fiber placed (AFP) composite parts.

Automated fiber placement (AFP) is one of two primary automated manufacturing methods used in the aerospace industry today, the other being automated tape laying which is similar to AFP but deposits bands of wider prepreg tape [5]. AFP employs a fiber placement head to align and deposit bands of narrow prepreg tape strips (referred to as tows with typical widths between roughly 3 mm and 13 mm), a roller to compact the tows on the tool surface, and an infrared heater to increase prepreg tack and provide some initial in situ consolidation [5-7]. One advantage of AFP is that it has the ability to fabricate complex parts with geometric features such as ply drops, cut-outs, and significant contours by clamping, cutting, restarting, and varying the deposition rate of individual tows [5, 8, 9]. Between 8 and 32 tows comprise one AFP band, and due to tow steering, gaps and overlaps are common manufacturing defects generated during layup that contribute to geometric and mechanical property variations [6, 10]. Even when a layup is programmed to have "zero-gap", tow overlaps can still occur. It has been shown that variation in tow width after the tape slitting process is a primary contributor to the gap/overlap variability in an AFP layup [10]. Therefore, in order to extend the previous thickness model's predictive capabilities for thickness-critical AFP parts, variations in slit tape prepreg properties and geometry were investigated in this study. Then, global sensitivity analysis was performed to understand the relative importance of input variations on AFP part thickness variability, and the AFP thickness model predictions were compared to measurements from production-scale representative parts in order to validate the model. In addition, since PPAW has been shown to be the primary predictor of hand layup unidirectional tape (unitape) part thickness when resin bleed is controlled, this study also investigated PPAW monitoring approaches to inform thickness model predictions [3].

2. THICKNESS MODEL REVISIONS AND FURTHER DEVELOPMENT

Since the introduction of the hand layup unitape thickness model in the previous study [3], there have been two important revisions to the model. The first revision involves the treatment of porosity (φ_{air}) in the thickness model expression (**Equation 1**), and the second allows for additional assumptions when considering the shrinkage and thermal strain that develop during cure. These are discussed in Sections 2.1 and 2.2, respectively. The ongoing development of the thickness model is being performed according to the Integrated Computational Materials Engineering (ICME) Verification and Validation (V&V) Guidelines [11, 12], which recognizes the iterative process of model development.

The biggest limitations of the validation activities in the previous study were the use of a qualitative validation approach, instead of a quantitative approach, and the fabrication of thin validation flat panels (8 plies) relative to production-scale parts [3]. Therefore, a critical step in further developing the hand layup unitape thickness model and extending the model's predictive capabilities to AFP parts involved quantitative validation of hand layup thickness predictions using measurements from production-scale representative parts. Then the model was calibrated for AFP part thickness predictions and subsequently validated using the same validation approach that was employed for the hand layup unitape thickness predictions. Additionally, global sensitivity analysis of the AFP thickness model was accomplished using the NESSUS® probabilistic analysis software [13].

2.1 Revised porosity in thickness model expression

One difference between the original and revised thickness model expression is the treatment of porosity. Porosity (φ_{air}) measurements of a cured part via acid digestion represent the residual void fraction in the part after consolidation and cure. Therefore, in the thickness model expression below the porosity modifies the entirety of the void-free, post-cure thickness prediction, as opposed to the original formulation in which the porosity does not modify the change in thickness due to shrinkage (Δt_{shrink}), thermal ($\Delta t_{thermal}$), and mechanical strain (Δt_{mech}). The revised model predicted thickness (t_{model}) is given by the following equation:

$$t_{model} = \frac{\dfrac{PPAW(1-RB)[\rho_r(1-RC)+\rho_f RC]}{\rho_f \rho_r} + \Delta t_{shrink} + \Delta t_{thermal} + \Delta t_{mech}}{(1-\varphi_{air})} \quad (1)$$

where $PPAW$ is the prepreg areal weight, RC is the resin content (wt%), ρ_f is the fiber density, ρ_r is the resin density, and RB is the resin bleed (wt%) during consolidation and cure.

2.2 Shrinkage and thermal strain assumptions

Shrinkage and thermal strain develop in a composite during cure due to the evolution of the resin cure shrinkage (CS) and the resin coefficient of thermal expansion (CTE), which are both a function of the resin degree of cure (x). The resin is a viscous fluid in the pre-gelation regime with a negligible elastic modulus compared to the fiberbed and no shear modulus, which means that resin flow is possible prior to gelation. In the case of a perfect resin dam, resin flow is restricted resulting in a buildup of hydrostatic pressure. Due to this hydrostatic pressure, the resin shrinkage and thermal strain contribute to the thickness of the composite prior to gelation and throughout the entirety of the cure cycle. The "perfect resin dam" assumption is in agreement with the original shrinkage and thermal strain formulations, in which the resin shrinkage and thermal strain were assumed to develop from the beginning of the cure cycle to the end of the cure cycle (**Equation 2**). However, if the resin is able to flow prior to gelation, such as in the case of no resin dam, then the resin and thermal shrinkage strain do not contribute to the thickness of the composite prior to gelation because the strain is non-recoverable and stress is carried by the solid fiberbed. After gelation, the resin is assumed to be an elastic solid and is stressed along with the fiberbed due to cure shrinkage and thermal expansion/contraction, which contributes to the thickness of the composite (**Equation 3**). The "perfect resin dam" and "no resin dam" assumptions are the bounding cases for the development of shrinkage and thermal strain during cure. The formulation for resin shrinkage (ε_{shrink}) and thermal strain ($\varepsilon_{thermal}$) development based on these two assumptions are given by the following equations:

Perfect Resin Dam: $$\varepsilon_{shrink} = \int_{x_i}^{x_f} CS(x)\, dx \qquad \varepsilon_{thermal} = \int_{T_i}^{T_f} CTE(x)\, dT \quad (2)$$

No Resin Dam: $$\varepsilon_{shrink} = \int_{x_{gel}}^{x_f} CS(x)\, dx \qquad \varepsilon_{thermal} = \int_{T_{gel}}^{T_f} CTE(x)\, dT \quad (3)$$

where x_i is the initial degree of cure, x_f is the final degree of cure, x_{gel} is the degree of cure at gelation, T_i is the initial temperature, T_f is the final temperature, and T_{gel} is the temperature at gelation

2.3 Parametric distributions of shrinkage, thermal, and mechanical strain

In order to understand the influence of shrinkage, thermal, and mechanical strain variations on part thickness variability, parametric distributions were approximated from probabilistic simulations. The probabilistic simulations for shrinkage and thermal strain involved identifying variations in the manufacturer recommended cure cycle, according to the resin technical data sheet (TDS), and using NESSUS® to compute the cumulative distribution function (CDF) from 2,000 Monte Carlo samples. The CDF was computed for both the "perfect resin dam" and "no resin dam" assumption, and then a probability density function was fit to the simulated distributions for the two assumptions separately and combined together. Combining the simulated distributions for the two assumptions together represents an "uncertain resin dam" situation. In other words, an "uncertain resin dam" situation is one in which a resin dam was used but resin bleed was not negligible. **Table 1** shows the cure cycle random variables based on information and ranges provided in the CYCOM® 5250-4 resin TDS [14].

Table 1. Random variable inputs to the thermal, shrinkage, and mechanical strain models

Cure Cycle Variables	Units	Source	Distribution	Parameters
Thermal and Shrinkage Strain Inputs				
Cure Ramp Rate	*°C/min*	resin TDS	uniform	*a*=0.6, *b*=3.0
Initial Hold Time	*min*	resin TDS	uniform	*a*=40, *b*=50
Cure Temperature	*°C*	resin TDS	uniform	*a*=177, *b*=204
Cure Hold Time	*min*	resin TDS	uniform	*a*=240, *b*=360
Post-cure Ramp Rate	*°C/min*	resin TDS	uniform	*a*=0.6, *b*=3.0
Post-cure Temperature	*°C*	resin TDS	uniform	*a*=191, *b*=243
Post-cure Hold Time	*min*	resin TDS	uniform	*a*=240, *b*=360
Mechanical Strain Inputs				
Autoclave Pressure at Gelation	*kPa*	resin TDS	uniform	*a*=100, *b*=586
Fiber Volume Fraction		estimated	uniform	*a*=0.58, *b*=0.625
Fiber Through-Thickness Modulus	*GPa*	estimated from fiber PDS	normal	μ=27.6, σ=4.14

Uniform probability density functions best described the shrinkage and thermal strain estimated from the probabilistic simulations. For shrinkage strain, the lower and upper bound parameters (*a* and *b* respectively) defining the uniform probability density functions were *a* = -0.013 and *b* = -0.011 for the "perfect resin dam" assumption, *a* = -0.011 and *b* = -0.008 for the "no resin dam" assumption, and *a* = -0.013 and *b* = -0.008 for the "uncertain resin dam" assumption. For thermal strain, the lower and upper bound parameters defining the uniform probability density functions were *a* = 0.012 and *b* = 0.016 for "perfect resin dam", *a* = -0.009 and *b* = -0.003 for "no resin dam", and *a* = -0.009 and *b* = 0.016 for the "uncertain resin dam" assumption.

Based on the mechanical strain formulation in the previous study [3], mechanical strain (ε_{mech}) due to autoclave pressure during cure is given by the following equation:

$$\varepsilon_{mech} = \frac{\frac{-P_{gel}}{\varphi_f}}{E_{33}} \tag{4}$$

where P_{gel} is the autoclave pressure at gelation, E_{33} is the through-thickness elastic modulus of the fiber, and φ_f is the volume fraction of fiber in the composite. The distributions for these random variables that were employed in the probabilistic simulation of mechanical strain are provided in **Table 1**. Using the recommended cure cycle, the pressure at gelation could range between 100 kPa (15 psi) and 586 kPa (85 psi). In general, the through-thickness modulus of carbon fiber is roughly one order of magnitude less than the elastic modulus in the fiber-direction (E_{11}). The elastic modulus of HexTow® IM7 carbon fiber in the fiber direction is listed as 276 GPa in the product data sheet (PDS) [15]. Therefore, the mean through-thickness elastic modulus was estimated to be 27.6 GPa, and a coefficient of variation of 15% was assumed, due to considerable uncertainty in the through-thickness modulus estimate. Additionally, the fiber volume fraction was estimated according to **Equation 5**. The lower and upper bound fiber volume fraction were calculated based on distributions for resin content (RC), fiber density (ρ_f), and resin density (ρ_r), and a uniform probability density function was used to describe the fiber volume fraction distribution based on the calculated lower and upper bound, which is a conservative assumption because uniform distributions ascribe an equal probability to all outcomes. After performing a full cumulative distribution probabilistic simulation with NESSUS®, a uniform probability density function was fit to the distribution of simulated mechanical strain values. The parameters of the uniform mechanical strain distribution were *a* = -7.8E-5 and *b* = -3.6E-6.

$$\varphi_f = \frac{\frac{(1-RC)}{\rho_f}}{\frac{(1-RC)}{\rho_f} + \frac{RC}{\rho_r}} \tag{5}$$

3. EXPERIMENTATION

3.1 Flat Panel Fabrication and Thickness Inspection

The intended use of the model is to predict the thickness of minimally contoured thickness critical composite parts. Therefore, flat panels were used as validation coupons, and, in order to achieve production-scale representative coupons, these flat panels were manufactured with a ply count of 40. A total of 8 hand layup unitape panels and 8 AFP panels were fabricated from multiple lots of prepreg made up of Cytec Solvay Group's CYCOM® 5250-4 curing bismaleimide (BMI) resin [14] and Hexcels's HexTow® IM7 carbon fiber [15]. Hand layup unitape plies were pattern cut from two lots of prepreg to a nominal area of 292.1 mm by 292.1 mm (11.5 in by 11.5 in) and were fabricated with a $[0/90]_{20}$ ply orientation. AFP flat panels were fabricated from five lots of 24-tow slit tape prepreg (with a nominal tow widths of 3.175 mm) to a nominal area of 457.2 mm by 609.6 mm (18 in by 24 in) with an orientation of $[0/90]_{20}$. Additionally, the AFP layup was programmed to have "zero-gap", and a band stagger that repeated every fifth ply was used to minimize the alignment of gaps and overlaps through the thickness of the layup. After layup all of the flat panels were vacuum bagged, and autoclave cured on aluminum tools without a caul, based on the resin manufacturer's recommended cure cycle [14]. Then the panels were debagged and thickness inspected using a Leica T-Scan laser inspection system manufactured by Hexagon Manufacturing Intelligence for high fidelity thickness measurements. The T-Scan laser inspection system generated a point cloud of thousands of thickness measurements, which were assumed to follow a normal distribution, and the mean and standard deviation of the measurements were calculated and reported. One limitation of this study is that T-Scan gauge error was not measured. Inputs to the thickness model were determined from the material certification (certs) package, the CYCOM® 5250-4 resin TDS [14], experimental measurements, and probabilistic simulations, which are specified below in **Table 2** and **Table 4**.

3.2 Model Validation Approach

The root mean square error (RMSE) of the average predicted ply thickness, as compared to the average measured ply thickness, of the 40-ply flat panels was the quantitative validation metric used in this study to determine the predictive capability of the model (**Equation 6**). The average predicted ply thickness was calculated using the mean of each random variable as an input to the thickness model and then dividing the predicted thickness by the number of plies in the flat panel. Thus, this approach is a deterministic validation of the thickness model's predictive capability. The predicted and measured ply thickness were also compared graphically by plotting the average measured ply thickness against the average predicted ply thickness with error bars representing plus or minus two times the RMSE, which is approximately a 95% confidence interval because RMSE is the standard deviation of the residuals. Thickness tolerance bounds of ±1.5% are displayed, in order to show the accuracy of the model predictions relative to thickness specification for high performance programs. Additionally, since PPAW has been reported to be one of the primary predictors of post-cure thickness, the correlation between the average measured thickness and average PPAW was examined via regression analysis.

$$RMSE = \sqrt{\frac{\sum(t_{predicted} - t_{measured})^2}{N}} \tag{6}$$

3.3 Prepreg Areal Weight Monitoring

Two slit tape PPAW monitoring methods were investigated in this study to inform the AFP thickness model. These methods are referred to as tow sampling and strip sampling. The tow sampling method involved extracting two slit tape samples from the head of the fiber placement machine before the start of the flat panel build and again after every tenth ply in the layup (for a total of 10 slit tape samples per 40-ply flat panel build). Then, the individual tows in the slit tape sample were straightened and cut to 2438.4 mm (96 in) (**Figure 1A**), the sample was weighed, and the PPAW of the sample was calculated by dividing the weight of the sample (m_{sample}) by the area of the sample, which is the length of the sample (l_{sample}) times the average tow width (w_{tow}) from the material certs times the number of tows (N_{tow}) (**Equation 7**). The strip sampling approach involved laying up a nominal 76.2 mm (3 in) wide by 609.6 mm (24 in) long strip of prepreg with the fiber placement machine next to the flat panel build during AFP fabrication

(**Figure 1B**). One ply of the strip sample was fiber placed at the beginning of the flat panel build and again after every fifth ply of the build. The PPAW of the strip was calculated by dividing the weight of the strip sample by the measured area multiplied by the number of plies in the sample.

$$PPAW_{TowSample} = \frac{m_{sample}}{l_{sample} \times w_{tow} \times N_{tow}} \tag{7}$$

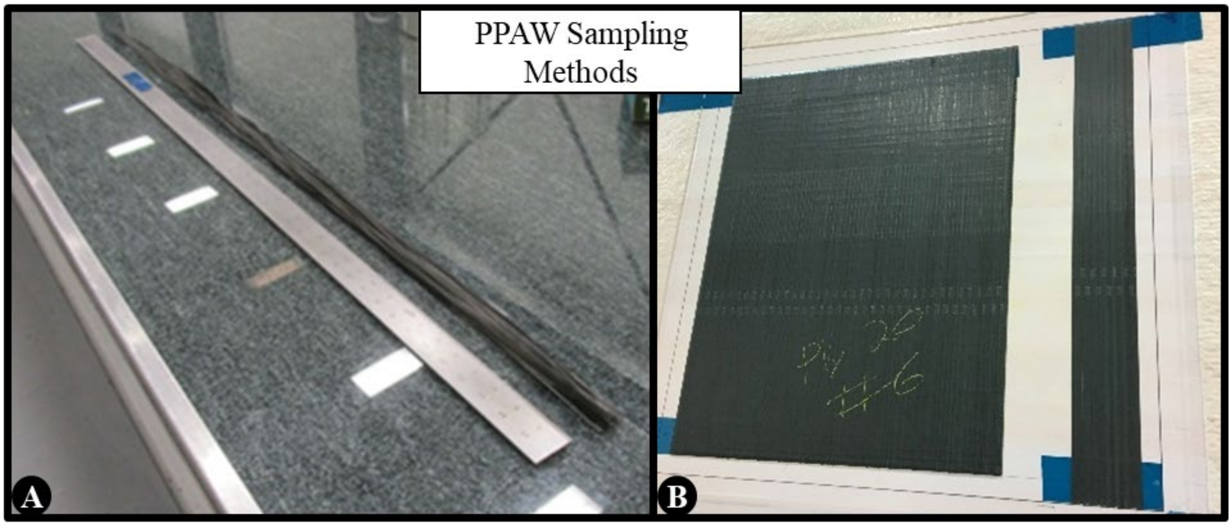

Figure 1. Prepreg areal weight (PPAW) sampling methods: (A) straightening and cutting a tow sample to length and (B) AFP flat panel with a strip sample to the right of the build

4. RESULTS AND DISCUSSION

4.1 Hand Layup Unitape Thickness Validation

The first step in extending the thickness model's predictive capabilities to AFP parts was to quantitatively validate the hand layup unitape thickness predictions. For the hand layup unitape flat panels, the PPAW of each ply was calculated by weighing the ply and dividing the weight by the measured area of the ply, in order to reduce uncertainty on the incoming material properties. Although the edges of the unitape flat panels were dammed and resin bleed was controlled to less than 1 wt%, notable edge effects (thin edges) were observed (**Figure 2A**). These thin edges were most likely caused by localized resin flow and bleed along the edges of the panel. Therefore, shrinkage and thermal strain distributions based on the "uncertain resin dam" assumption were used as inputs to the thickness model. Additionally, the mechanical strain distribution estimated via probabilistic simulation in Section 2.3 was used as an input to model. The remaining input variable distributions were carried over from the previous study [3], under the assumption that resin bleed is controlled (≤ 1 wt%), and are listed in **Table 2**.

An example of a T-Scan thickness inspection map of a hand layup flat panel is shown in **Figure 2A**. A specific consequence of the observed edge effects could be a slight reduction in the average measured ply thickness. **Figure 2B** shows a plot comparing the average measured ply thickness to the average predicted ply thickness. All eight of the ply thickness predictions were within 1.5% of the measured thickness and, when accounting for the RMSE, all but one of the thickness predictions were within the tolerance bounds with 95% confidence.

Table 2. Random variable inputs to the hand layup unitape thickness model

Unitape Thickness Variables	Units	Source	Distribution	Parameters
Incoming Material Inputs				
Prepreg Areal Weight ($PPAW$)	g/m^2	individual ply measurements	deterministic	
Resin Content (RC)	*wt%*	material certs	normal	μ=31.720, σ=0.529
Fiber Density (ρ_f)	*g/cc*	material certs	normal	μ=1.781, σ=0.003
Resin Density (ρ_r)	*g/cc*	estimated COV = 0.5%	normal	μ=1.250, σ=0.006
Part-Manufacturing Inputs				
Resin Bleed (RB)	*wt%*	resin TDS	uniform	*a*=0, *b*=1
Porosity (φ_{air})	*vol%*	acid digestion of panels	uniform	*a*=0, *b*=1.215
Cure Shrinkage Strain (ε_{shrink})	*mm/mm*	"uncertain resin dam"	uniform	*a*=-0.013, *b*=-0.008
Thermal Strain ($\varepsilon_{thermal}$)	*mm/mm*	"uncertain resin dam"	uniform	*a*=-0.009, *b*=0.016
Mechanical Strain (ε_{mech})	*mm/mm*	probabilistic simulations	uniform	*a*=-7.8E-5, *b*=-3.6E-6

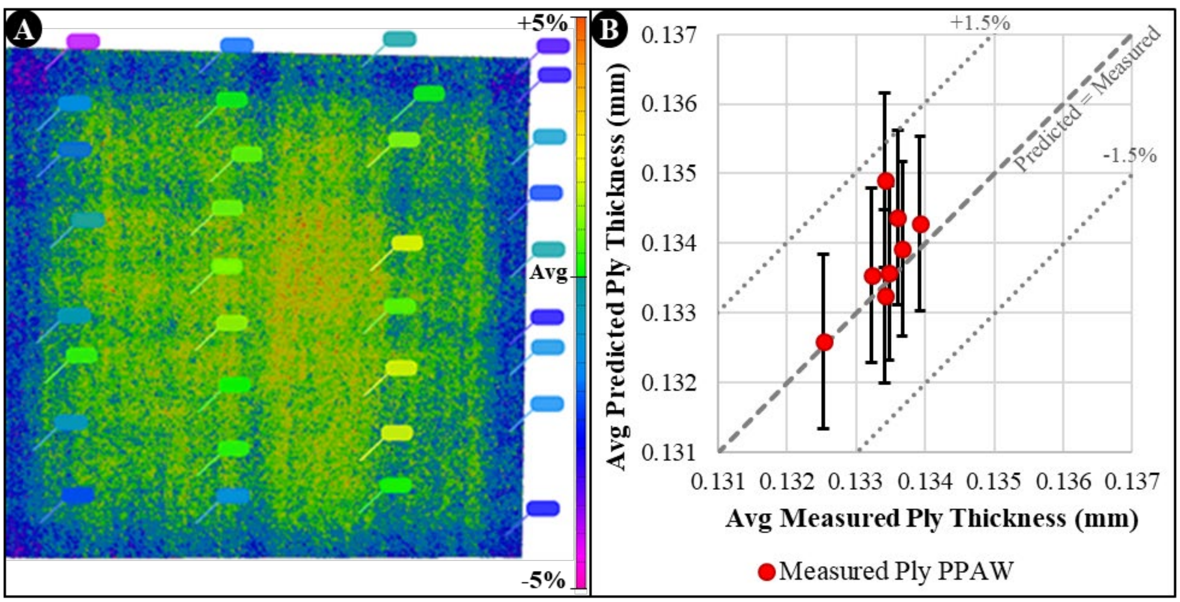

Figure 2. Hand layup unitape thickness inspection and validation: (A) example T-Scan thickness inspection map of Panel 5 and (B) predicted versus measured ply thickness of flat panels

The average PPAW from the 40 individual ply measurements, the average measured ply thickness from the T-Scan inspection, and the average model predicted ply thickness are shown in **Table 3** below, along with the RMSE of the model predictions and the R^2 value of the correlation between the measured ply thickness and the PPAW. The RMSE of the average predicted ply thickness was 6.26E-4 mm, which is equivalent to 0.025 mm for 40-ply panel thickness. The correlation between measured thickness and PPAW was weaker than expected with an R^2 value of only 0.509. The RMSE was dominated by Panel 8, and further examination showed that the relationship between the measured ply thickness and the average PPAW for Panel 8 was not in line with the other panels. Therefore, Chauvenet's exclusion criterion was employed to determine if the measured thickness of Panel 8 was a potential outlier [16]. Based on a comparison of measured thickness to PPAW ratios, the measured thickness of Panel 8 could be excluded according to Chauvenet's criterion. If Panel 8 was excluded, then the RMSE of a single ply would reduce by almost half to 3.6E-4 mm (0.014 mm for 40-ply panel thickness), and the R^2 value representing the correlation between the measured thickness and PPAW would improve to 0.807. These validation activities provided a quantitative metric (RMSE) of the predictive capability of the thickness model, and the predicted versus measured results showed good agreement for extending the model to AFP thickness prediction.

Table 3. Hand layup unitape 40-ply flat panel validation data

Panel Number	Avg. PPAW (g/m^2)	Avg. Measured Ply Thickness (mm)	Avg. Predicted Ply Thickness (mm)
1	210.052	0.13348	0.13358
2	211.147	0.13392	0.13427
3	208.491	0.13252	0.13258
4	209.514	0.13341	0.13323
5	209.979	0.13322	0.13353
6	210.591	0.13367	0.13392
7	211.296	0.13360	0.13437
8	212.141	0.13341	0.13491
Measured Thickness vs. PPAW	R^2 = 0.509		
RMSE (mm)			**6.26E-4**

4.2 Automated Fiber Placement Thickness Calibration and Sensitivity Analysis

Initially, the unitape hand layup thickness model was used to predict the average ply thickness of AFP flat panels using the average PPAW from the material certs, the tow sampling method, and the strip sampling method (**Figure 3A**). This was done in order to understand the preliminary accuracy of the model for AFP thickness prediction and to guide the calibration activities. The average AFP ply thickness predictions based on the tow sampling and strip sampling PPAW methods appeared to be significantly accurate without calibration to accommodate for the additional uncertainty introduced by the AFP process. However, the average ply thickness predictions based on the material certs were approximately 0.004 mm (3.2%) thicker compared to the average measured ply thickness. Interestingly, the relationship between the average measured ply thickness and the average PPAW revealed that the PPAW reported in the material certs was larger than the measured PPAW from the tow sampling and strip sampling methods (**Figure 3B**). In fact, the average tow sampling and strip sampling PPAW was 203.572 and 203.702 g/m^2 respectively, and the average material cert PPAW was 210.675 g/m^2, which is approximately 3.3% to 3.4% greater than the measured PPAW. Thus, the discrepancy in the reported versus measured PPAW was the primary source of the error in the thickness predictions based on the material certs. The material certs report the PPAW of the prepreg tape prior to slitting, whereas the PPAW measurements are taken after the tape slitting process. Therefore, the tape slitting process was identified as the most likely cause of the PPAW discrepancy. The reduction in area, resin transfer from the prepreg to the slitting machine rollers, and resin bleed due to compaction are all possible phenomena responsible for reducing the PPAW during tape slitting.

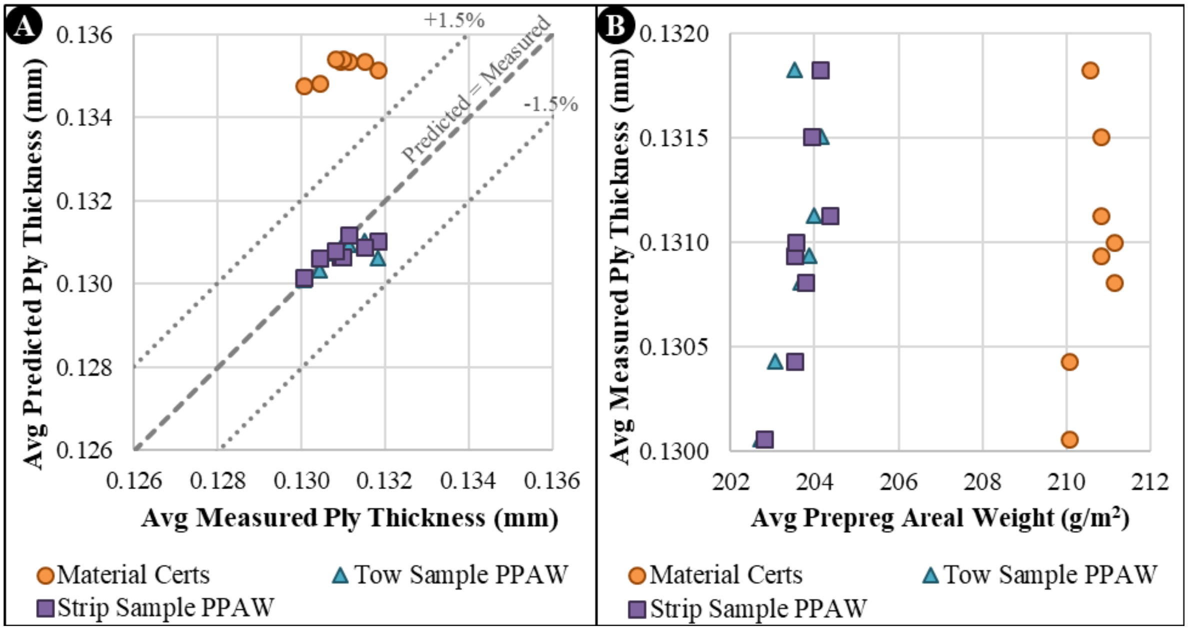

Figure 3. Preliminary AFP results by prepreg areal weight source: (A) predicted versus measured ply thickness and (B) relationship between measured ply thickness and prepreg areal weight

In order to represent the slit tape PPAW in the thickness model, a calibrated factor was needed to reduce the incoming PPAW reported by the material certs. The PPAW from the tow sampling method was used as the calibration measurements because the tow sampling method did not include additional AFP processing, as opposed to the PPAW measurements from the strip sampling approach. According to **Equation 7**, the weight of the tow samples were divided by the length of the sample (2438.4 mm) times the number of tows (24) times the width of the tows, which was treated as a random variable (normal distribution: μ=3.173, σ=0.039) based on the tow widths that are reported in the material certs after the slitting process. A probabilistic simulation was performed with NESSUS®, in order to estimate the PPAW distribution after slitting, which followed a normal distribution with a mean of 203.709 and standard deviation of 0.841 g/m^2. Randomly sampling the post-slitting PPAW distribution ($PPAW_{TowSample}$) and the pre-slitting PPAW distribution ($PPAW_{Certs}$) from the material certs (normal: μ=210.393, σ=1.310) for different probability percentiles, the distribution of the slit tape factor (F_{slit}) was estimated based on **Equation 8**. Thus, it was possible to compute the PPAW after slitting ($PPAW_{slit}$) based on the PPAW reported in the material certs and the calibrated slit tape factor, according to **Equation 9**.

$$F_{slit} = \frac{PPAW_{Certs} - PPAW_{TowSample}}{PPAW_{Certs}} \tag{8}$$

$$PPAW_{slit} = PPAW_{Certs}(1 - F_{slit}) \tag{9}$$

Table 4. Random variable inputs to the AFP thickness model

AFP Thickness Variables	Units	Source	Distribution	Parameters
Incoming Material Inputs				
Prepreg Areal Weight ($PPAW$)	*g/m²*	material certs	normal	μ=210.393, σ=1.310
Resin Content (RC)	*wt%*	material certs	normal	μ=31.386, σ=0.361
Fiber Density (ρ_f)	*g/cc*	material certs	normal	μ=1.781, σ=0.003
Resin Density (ρ_r)	*g/cc*	estimated COV = 0.5%	normal	μ=1.250, σ=0.006
Slit Tape Factor (F_{slit})	*wt%*	tow sample measurements	normal	μ=3.176, σ=0.202
Part-Manufacturing Inputs				
Resin Bleed (RB)	*wt%*	breather cloth measurements	uniform	a=0, b=0.5
Porosity (φ_{air})	*vol%*	acid digestion of panels	lognormal	μ=1.038, σ=0.239
Cure Shrinkage Strain (ε_{shrink})	*mm/mm*	"perfect resin dam"	uniform	a=-0.013, b=-0.011
Thermal Strain ($\varepsilon_{thermal}$)	*mm/mm*	"perfect resin dam"	uniform	a=0.012, b=0.016
Mechanical Strain (ε_{mech})	*mm/mm*	probabilistic simulations	uniform	a=-7.8E-5, b=-3.6E-6

The AFP thickness model is expressed in **Equation 10** and the AFP input variable distributions to the model are shown in **Table 4**. The input variable distributions for PPAW, resin content, and fiber density were determined from the material certs. The resin density was estimated to have a coefficient of variation (COV) of 0.5%, which is a conservative estimate because it is three times greater than fiber COV, and a mean of 1.25 g/cc from the resin TDS [14]. The resin bleed and acid digestion were determined from the 40-ply AFP flat panels. Resin bleed was calculated based on the increase in breather cloth weight after cure and was less than 0.5% for all of the panels. Edge effects due to resin bleed were not observed for the AFP panels, thus the shrinkage and thermal strain distributions based on the "perfect resin dam" assumption were used as inputs to the thickness model. The porosity distribution was determined from acid digestion void fraction measurements of the AFP flat panels.

Global sensitivity analysis shows the relative influence of the input distributions on the AFP thickness variability in the model predictions (**Figure 4**). These results continue to point to PPAW (global sensitivity = 0.68) as the primary predictor of thickness and thickness variability when resin bleed is controlled. Porosity and slit tape factor variations are the next two most important factors with global sensitivities of 0.10 and 0.07 respectively. A limitation of this study is that the calibration activities did not involve the investigation of thickness variability as a function of programmed gap/overlap or band stagger technique. However, the reduction in PPAW due to the tape slitting process appears to be the first-order phenomena that introduces additional variations in the AFP process, which is further indicated by the strong sensitivity of AFP thickness to PPAW. Furthermore, note that gaps and overlaps are strongly sensitive to variations in the tow widths, which is captured by the slit tape factor distribution [10].

$$t_{model} = \frac{\frac{PPAW(1-RB)\left[\rho_r(1-RC)+\rho_f RC\right]}{\rho_f \rho_r}(1-F_{slit}) + \Delta t_{shrink} + \Delta t_{thermal} + \Delta t_{mech}}{(1-\varphi_{air})} \quad (10)$$

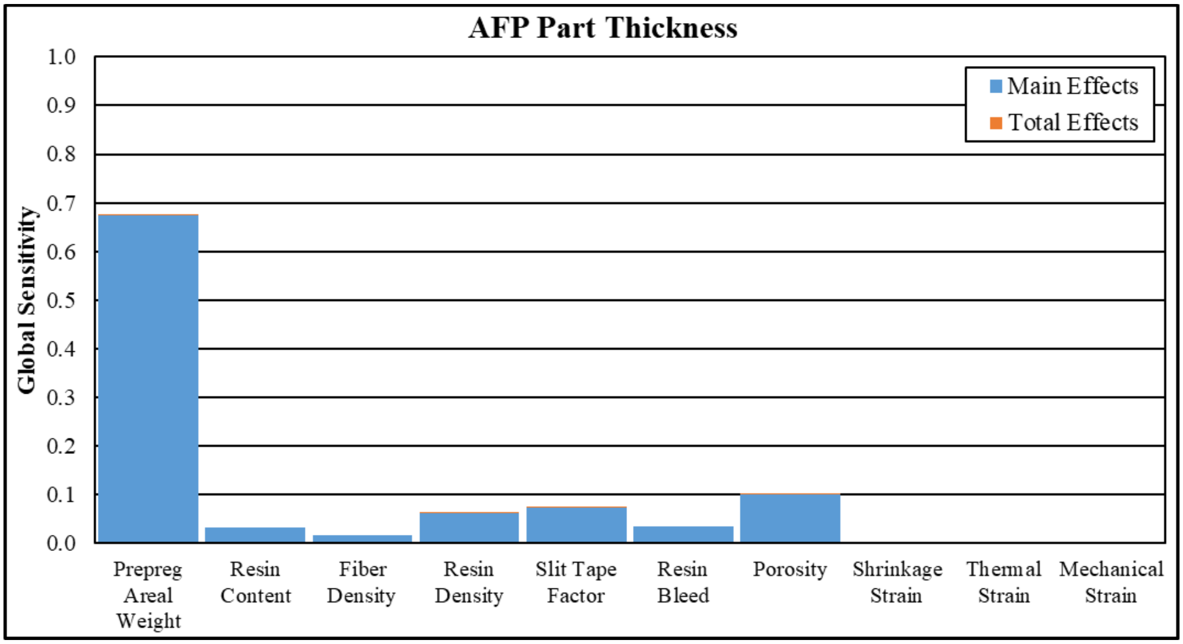

Figure 4. Global sensitivity analysis of the AFP thickness model

4.3 Automated Fiber Placement Thickness Validation

After model calibration the average measured ply thickness was plotted against the average predicted ply thickness based on the PPAW reported in the material certs and adjusted by the slit tape factor (**Figure 5A**). The adjusted material certs thickness prediction was significantly more accurate, in fact, all eight of the thickness predictions were within ±1.5% of the measured thickness with 95% confidence. The other thickness predictions based on the tow sampling method (**Figure 5B**) and the strip sampling method (**Figure 5C**) were accurate as well. All of the strip sampling thickness predictions and tow sampling thickness predictions were within the tight 1.5% thickness tolerance bounds with a 90% confidence, and all but one (Panel 2 tow sampling thickness prediction) were within the tolerance bounds with a 95% confidence. The AFP flat panels did not exhibit significant edge effects, but there was noticeable quilting, which is the checkered pattern on the surface of the panel caused by the gap/overlap associated with the band staggering technique (**Figure 5D**). In this study, it was assumed that the quilting pattern did not have a significant effect on the average measured thickness via T-Scan inspection because the thick and thin regions should average out in the inspection (especially given that resin bleed was negligible). The quilting pattern did increase the variability in the thickness measurements, however, the ability of the thickness model to predict thickness variability was not evaluated in this study. It is also important to note that the quilting observed on the AFP flat panels is most likely more pronounced than what is observed in production because more elaborate ply orientations are employed in production to prevent overlapping of the band stagger.

The RMSE for AFP ply thickness predictions (shown in **Table 5**) was less than that of the unitape hand layup ply thickness prediction (**Table 3**). The RMSE of the material certs (with adjustment for the slit tape reduction in PPAW), the tow sampling, and strip sampling ply thickness predictions were 4.30E-4 mm (0.017 mm for 40-ply panel thickness), 4.76E-4 (0.019 mm for 40-ply panel thickness), and 4.01E-4 (0.016 mm for 40-ply panel thickness) respectively.

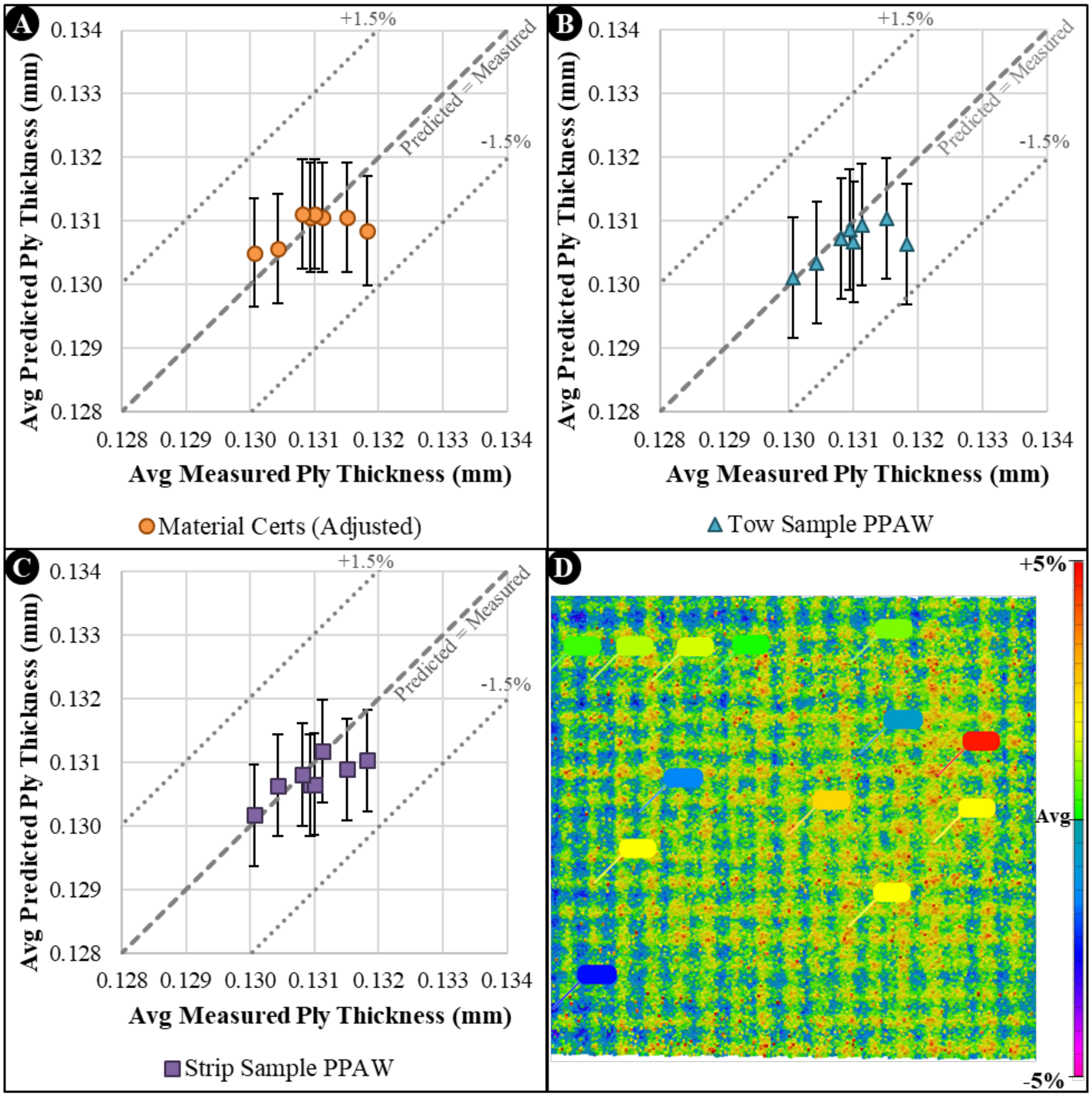

Figure 5. AFP validation and thickness inspection: (A) material certs predicted vs. measured thickness, (B) tow sampling predicted vs. measured thickness, (C) strip sampling predicted vs. measured thickness, and (D) example T-Scan thickness inspection map of Panel 3

However, the correlation between measured thickness and PPAW was still weaker than expected, with the strongest R^2 value being 0.644 for the strip sampling PPAW. Similar to the unitape hand layup flat panels, there is one panel in particular that dominates the RMSE computation: Panel 2. Again, using Chauvenet's criterion for exclusion based on the ratio of the measured thickness to PPAW reveals that the average measured thickness of Panel 2 could be considered an outlier [16]. Excluding Panel 2 from the dataset, would reduce the RMSE to 2.77E-4 mm, 2.35E-4 mm, and 3.04E-4 mm for the adjusted material certs, tow sampling, and strip sampling ply thickness predictions respectively. Additionally, the correlation R^2 value between the tow sampling PPAW and measured thickness would increase to 0.927, and the adjusted material certs R^2 value would improve to 0.542. The strip sampling R^2 value would remain relatively unchanged at 0.623.

Table 5. AFP 40-ply flat panel validation data

		Material Certs (Adjusted)		Tow Sample PPAW		Strip Sample PPAW	
Panel Number	**Avg. Measured Ply Thickness (mm)**	Avg. PPAW (g/m²)	Avg. Predicted Ply Thickness (mm)	Avg. PPAW (g/m²)	Avg. Predicted Ply Thickness (mm)	Avg. PPAW (g/m²)	Avg. Predicted Ply Thickness (mm)
1	0.13006	203.385	0.13051	202.709	0.13011	202.794	0.13017
2	0.13183	203.863	0.13086	203.519	0.13063	204.135	0.13103
3	0.13094	204.124	0.13106	203.875	0.13086	203.537	0.13064
4	0.13151	204.124	0.13106	204.157	0.13104	203.917	0.13089
5	0.13113	204.124	0.13106	203.998	0.13094	204.367	0.13118
6	0.13100	204.425	0.13111	203.580	0.13067	203.554	0.13065
7	0.13043	203.403	0.13056	203.069	0.13034	203.527	0.13064
8	0.13081	204.425	0.13111	203.667	0.13073	203.789	0.13081
Measured Thickness vs. PPAW		$R^2 = 0.246$		$R^2 = 0.526$		$R^2 = 0.644$	
RMSE (mm)			**4.30E-4**		**4.76E-4**		**4.01E-4**

5. CONCLUSIONS

In this study, the unitape hand layup thickness model and the automated fiber placement thickness model for thickness critical autoclave composites were quantitatively validated using the root mean square error metric. The test coupons used to validate the model were 40-ply flat panels, which are representative of minimally contoured production-scale parts, and the root mean square error of the ply thickness predictions were ≤ 6.26E-4 mm (≤ 0.025 mm for 40-ply panel thickness) for both validation cases. All of the average thickness predictions were within the specified ±1.5% thickness tolerance and most of their 95% confidence bounds were as well. A significant finding of this study is that the tape slitting process reduces the prepreg areal weight (PPAW) by roughly 3.2% on average, and is the primary difference between unitape hand layup and AFP thickness development. Despite additional sources of variability and uncertainty introduced by the AFP process, PPAW remains the primary predictor of cured part thickness when resin bleed is controlled. Interestingly, the same thickness model can be used to predict hand layup unitape and AFP part thickness, when monitored PPAW is provided as an input to the model, instead of the PPAW from the slit tape material certs. However, the correlations between measured thickness and PPAW were weaker than expected, unless potentially outliers were removed (max R^2 before removing potential outliers = 0.644; max R^2 after removing potential outliers = 0.927), which may not be fully justified given the size of the dataset. PPAW monitoring methods were used to calibrate the PPAW correction factor for the tape slitting process (F_{slit}) and showed some potential to improve model predictions, but a separate study is needed to investigate an optimum PPAW monitoring approach to significantly improve model predictions. Given the sensitivity of the predicted thickness to PPAW, an optimized monitoring approach could also reduce thickness variability. Future work will entail a probabilistic validation of the thickness model, in order to evaluate the capability of the model to predict thickness variability.

6. ACKNOWLEDGEMENT

The authors wish to acknowledge the funding support for this work from the Air Force Research Laboratory, Materials and Manufacturing Directorate, Manufacturing and Industrial Technologies Division under Contract FA8650-15-C-5707.

7. REFERENCES

[1] S. Zhang, L. Zhang, Y. Wang, J. Tao, and X. Chen, "Effect of ply level thickness uncertainty on reliability of laminated composite panels," *Journal of Reinforced Plastics and Composites,* vol. 35, no. 19, pp. 1387-1400, 2016. https://doi.org/10.1177/0731684416651499

[2] T. Mesogitis, A. Skordos, and A. Long, "Uncertainty in the manufacturing of fibrous thermosetting composites: A review," *Composites Part A: Applied Science and Manufacturing,* vol. 57, pp. 67-75, 2014. https://doi.org/10.1016/j.compositesa.2013.11.004

[3] M. Kirby, D. Riha, C. Madsen, C. Deemer, and B. Volk, "Development of a Semi-analytical Model for Predicting Thickness of Critical Autoclave Composites," presented at the CAMX, Dallas, TX, October 15-18, 2018.

[4] M. Elkington, D. Bloom, C. Ward, A. Chatzimichali, and K. Potter, "Hand layup: understanding the manual process," *Advanced Manufacturing: Polymer & Composites Science,* vol. 1, no. 3, pp. 138-151, 2015/07/03 2015. https://doi.org/10.1080/20550340.2015.1114801

[5] H.-J. L. Dirk, C. Ward, and K. D. Potter, "The engineering aspects of automated prepreg layup: History, present and future," *Composites Part B: Engineering,* vol. 43, no. 3, pp. 997-1009, 2012. https://doi.org/10.1016/j.compositesb.2011.12.003

[6] K. Croft, L. Lessard, D. Pasini, M. Hojjati, J. Chen, and A. Yousefpour, "Experimental study of the effect of automated fiber placement induced defects on performance of composite laminates," *Composites Part A: Applied Science and Manufacturing,* vol. 42, no. 5, pp. 484-491, 2011. https://doi.org/10.1016/j.compositesa.2011.01.007

[7] P. Debout, H. Chanal, and E. Duc, "Tool path smoothing of a redundant machine: Application to Automated Fiber Placement," *Computer-Aided Design,* vol. 43, no. 2, pp. 122-132, 2011. https://doi.org/10.1016/j.cad.2010.09.011

[8] L. Izco, J. Isturiz, and M. Motilva, "High speed tow placement system for complex surfaces with cut/clamp/& restart capabilities at 85 m/min (3350 IPM)," SAE Technical Paper, 0148-7191, 2006. https://doi.org/10.4271/2006-01-3138

[9] R. DeVlieg, K. Jeffries, and P. Vogeli, "High-speed fiber placement on large complex structures," SAE Technical Paper, 0148-7191, 2007. https://doi.org/10.4271/2007-01-3843

[10] M. Y. Matveev, F. G. Ball, I. A. Jones, A. C. Long, P. J. Schubel, and M. Tretyakov, "Uncertainty in geometry of fibre preforms manufactured with Automated Dry Fibre Placement and its effects on permeability," *Journal of Composite Materials,* p. 0021998317741951, 2017. https://doi.org/10.1177/0021998317741951

[11] B. Cowles, D. Backman, and R. Dutton, "Verification and validation of ICME methods and models for aerospace applications," *Integrating Materials and Manufacturing Innovation,* vol. 1, no. 1, p. 2, 2012. https://doi.org/10.1186/2193-9772-1-2

[12] B. A. Cowles, D. G. Backman, and R. E. Dutton, "Update to recommended best practice for verification and validation of ICME methods and models for aerospace applications," *Integrating Materials and Manufacturing Innovation,* vol. 4, no. 1, p. 2, 2015. https://doi.org/10.1186/s40192-014-0030-8

[13] "NESSUS User Manual," Southwest Research Institute, San Antonio, TX, 2015.

[14] Cytec Solvay Group, "CYCOM 5250-4 Prepreg System," Technical Data Sheet, Mar. 2012 [Rev 01].

[15] Hexcel Corporation, "HexTow IM7 Carbon Fiber," Product Data Sheet, 2018.

[16] J. P. Holman, *Experimental methods for engineers*, McGraw-Hill, New York, NY, 2012.